Novel inspection of welded joint microstructure using magneto-optical imaging technology*

Xiang-dong Gao(高向东)[1,†], Zheng-wen Li(李正文)[1], De-yong You(游德勇)[1], and Seiji Katayama[2]

[1] School of Electromechanical Engineering, Guangdong University of Technology, Guangdong 510006, China
[2] Joining and Welding Research Institute, Osaka University, 11-1 Mihogaoka, Ibaraki, Osaka 567-0047, Japan

(Received 11 November 2016; revised manuscript received 5 January 2017; published online 30 March 2017)

A novel method for measuring differences of microstructure by advanced use of the Faraday magneto-optical effect is proposed. Two groups of YAG laser welds on Q235 have been investigated in order to compare MO imaging and traditional methods. Microstructure images have been compared with MO images, and MO diagrams display different colors and gray scales for the base metal, the weld zone, and the heat affected zone. Experimental results indicate that the welded joint microstructure can be inspected by MO imaging without metallographic preparation.

Keywords: welded joint inspection, microstructure property, magneto-optical imaging

PACS: 42.62.–b, 78.20.Ls, 81.20.Vj **DOI:** 10.1088/1674-1056/26/5/054214

1. Introduction

Laser welding is a complicated technique with wide applications in manufacturing.[1,2] During welding, various microstructures inevitably occur, caused by different welding parameters, and the properties of metal materials after welding, such as strength, toughness, and thermal input tend to be affected by their microstructure. Hence, differences in microstructure play a crucial role in evaluating quality after welding.[3,4] Several techniques have been employed during the last few decades as efficient methods to reveal the microstructure of the weldment, e.g., classical metallographic grain analysis based on chemically etched surfaces with scanning acoustic microscopy,[5] metallographic microscopy, and scanning electron microscopy methods,[6] as well as detection by electron beam scattering diffraction and x-ray diffraction imaging.[7,8] In this article, a novel magneto-optical (MO) imaging detection method of analysis by Faraday MO effect is proposed and experimented.[9,10]

The Faraday MO effect is a phenomenon in which polarization of incident light is rotated to an angle θ under the effect of an external magnetic field.[11,12] The angle θ can be described as

$$\theta = VBL, \tag{1}$$

where V is the Verdet constant of the medium, B represents the magnetic induction intensity in the direction of light propagation, and L represents the optical path by which the light travels through the magnetic medium.

A schematic diagram of the experimental setup is shown in Fig. 1. As can be observed, the MO sensor is installed on top of the detected weldment to obtain MO images. The direct-current electromagnet is placed under the weldment to generate the magnetic field. The mechanism of MO imaging can be described as below.

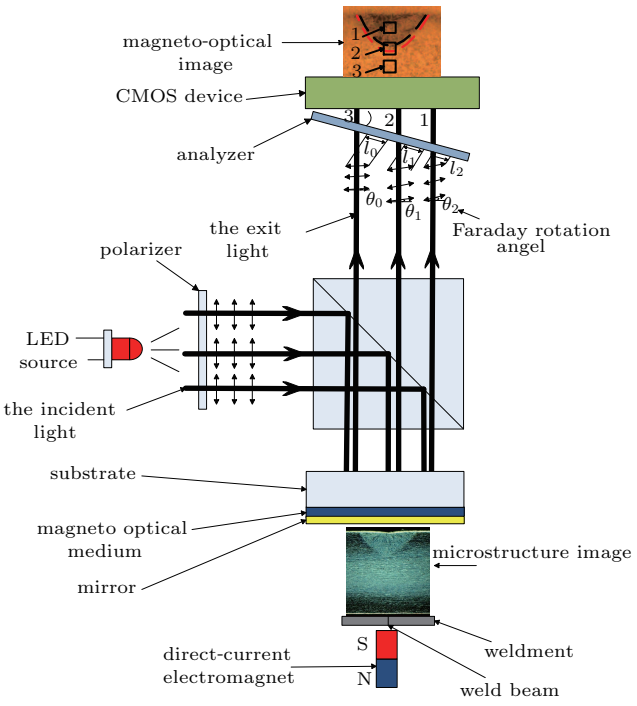


Fig. 1. (color online) Schematic diagram of magneto-optical imaging.

The incident light is emitted by a light emitting diode (LED) and is polarized when passing through a polarizer. The weldment is magnetized by the direct-current electromagnet, and the induced magnetic fields change the magnetic state of

*Project supported by the National Natural Science Foundation of China (Grant No. 51675104), the Science and Technology Planning Project of Guangzhou, China (Grant No. 201510010089), and the Science and Technology Planning Public Project of Guangdong Province, China (Grant No. 2016A010102015).

†Corresponding author. E-mail: gaoxd666@126.com

© 2017 Chinese Physical Society and IOP Publishing Ltd

the MO film. As the polarized light passes through the substrate and active MO medium twice, a Faraday rotation is produced in the polarized light. Then the polarized light is analyzed by the analyzer placed in the path of the exiting light, and lastly the optical contrast corresponding to the rotation is captured by an imaging device (CMOS camera). Only when the magnetic field direction is parallel to the direction of the incident light can a rotation be induced in the polarized light, and the variation of brightness can show up in an MO image.

When the linearly polarized light passes through the MO film where the magnetic field exists, the amplitude of the linearly polarized light projected on the analyzer can be described as

$$L = E\cos\varphi, \tag{2}$$

where E is the amplitude of the linearly polarized light, and φ is the angle between the CMOS device and the analyzer.

The corresponding light intensity I_i ($i = 0, 1, 2$) can be expressed as

$$I_0 = E^2\cos^2(\varphi + \theta_0), \tag{3}$$

$$I_1 = E^2\cos^2(\varphi + \theta_1), \tag{4}$$

$$I_2 = E^2\cos^2(\varphi + \theta_2). \tag{5}$$

The corresponding regions in the MO image of I_i ($i = 0, 1, 2$) are shown in Fig. 1. The light intensities I_0, I_1, and I_2 in the MO images appear in orange, brown, and black, respectively, and they represent regions 1, 2, and 3.

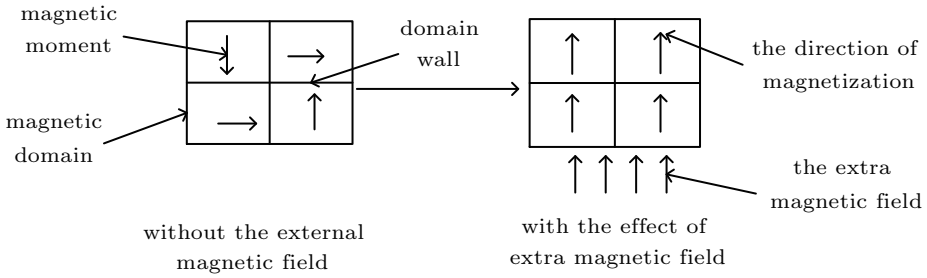


Fig. 2. Theory of magnetic domain.

Q235 is a kind of ferromagnetic material whose element atoms have quite a strong magnetic moment. As shown in Fig. 2, a spontaneous magnetization area, called the magnetic domain, based on the quantum theory of Weiss is easily formed.[13] Moreover, the direction of each magnetic domain is different in every atom, however the effect of the entire magnetic domain is offset reciprocally. In general, no magnetism is exhibited. The material is magnetized only when affected by an external magnetic field.

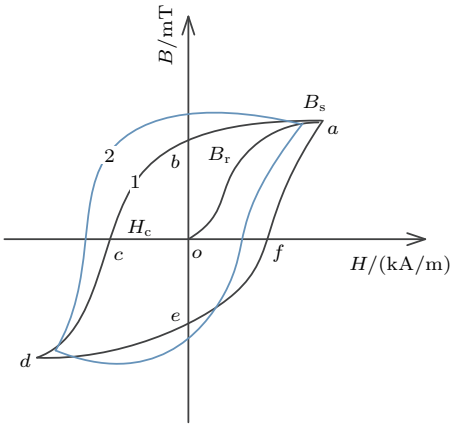


Fig. 3. (color online) Hysteresis loop. The change from curve 1 to curve 2 represents the grain size decreasing.

As the intensity of the external magnetic field H increases from 0, the magnetization intensity B of the weldment is gradually enhanced. As shown in Fig. 3, a curve that reflects the variation tendency between magnetization intensity B and magnetic intensity H is called a hysteresis loop.[14] And B can be expressed as

$$B = \mu H, \tag{6}$$

where μ is the permeability of the material. In the magnetization process, when H increases, B increases dramatically at first and then more slowly until it reaches saturated magnetization intensity B_s. However, when H decreases, B changes along curve ab instead of curve oa. Although H reduces to zero along curve ad, residual magnetism B_r remains in the material. A reverse magnetic field is added to eliminate the residual magnetism B_r. When it increases to H_c, B turns to zero, and H_c is called coercivity.[15] A large coercivity signifies a high residual magnetism.[16,17] Meanwhile, if the reverse magnetic field decreases, B increases in the opposite direction till it reaches the saturated intensity. When the magnetic intensity changes again along curve da, the change of the magnetization intensity is symmetrical to the anterior change. Finally, a closed curve called the hysteresis loop is caused. Hysteresis is the unique phenomenon of ferromagnetic materials that reveals the irreversibility of the magnetization process.

There is a great deal of difference between the welded joint and the base steel after welding. The welded joint can be classified to one of several zones based on differences of microstructure.[18–20] MO imaging on account of materials'

electromagnetic properties is an effective method to identify those differences.

2. Experiments

2.1. Material and welding parameters

Metal material Q235 with a length of 100 mm, width of 60 mm, and thickness of 2 mm was welded by an Nd: YAG laser welding equipment under argon atmosphere with a flux of 27 L/min. The chemical composition of Q235 is shown in Table 1. Alcohol and acetone were used before the welding to remove dust and impurities from the weldment surface. The weldment was cut into conveniently sized samples of 30 mm×25 mm×2 mm to obtain desirable etching and grinding results. All the weldments were classified into group A and group B. The laser welding parameters of each group, including the average power, peak power, speed, pulse duration, pulse frequency, and defocusing, are displayed in Table 2. Then the differences of microstructure resulting from different welding conditions were compared.

Table 1. Chemical composition of Q235 (wt.%).

C	Si	Mn	P	S	Nb	B
14	19	55	2.8	2.0	Remain	

Table 2. Welding parameters of groups A and B.

	Average power/W	Peak power/kW	Speed /(m/min)	Pulse duration/ms	Defocusing /mm	Pulse frequency/Hz
A	64	2	3	5	1	4
B	96	3	3	5	1	4

2.2. Experimental setup of MO image acquisition

As can be seen in Fig. 4, the experimental setup consists of a portal frame, a base plate, a manual moving table, a two-axis moving experimental platform equipped with servo motors, two fixtures, and an MO image collector. The MO sensor and the weldment were fixed separately in the experimental setup. MO images were captured by the image collector.

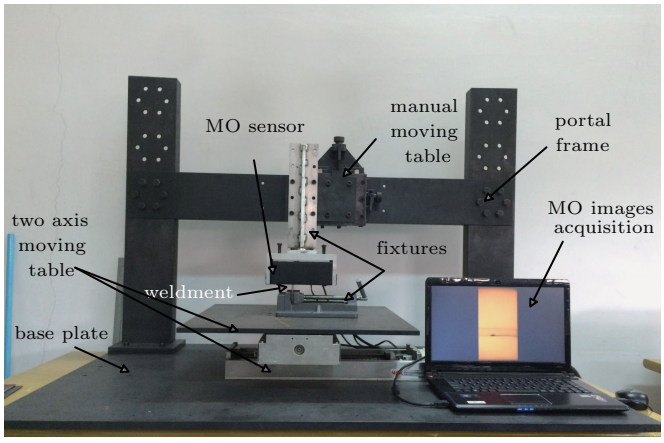


Fig. 4. (color online) Experimental setup to detect microstructure of welded joint using magneto-optical imaging technology.

2.3. Microstructure of weldment and MO imaging tests

The experiments of butt plate welding were performed with an Nd:YAG laser welding machine. Weldments were cut by a metallographic cutting machine. As the metallographic specimens, the polished weldments were etched by using a solution of 1 ml nitric acid and 19 ml ethanol. Furthermore, the weldment's microstructure was investigated by the optical microscope. The MO setup was employed to acquire MO images of the welded joint section and surface.

3. Results and discussion

In Fig. 5, comparison diagrams of different regions (1, 2, 3) of weldment A are shown, including the MO images of the welded joint surface and section and the microstructure images of the section. Toward images of the welded joint surface, because the average power was low and the welding speed was slow, good appearance can be observed in the real image of the weldment. Three regions (regions 1, 2, 3) are found in the MO image and the selected MO images. As the findings show, region 1 is dark brown and represents the weld zone (WZ). Two parts of region 3 are deep orange, and there was base metal. Region 2 indicates that heat affected zones exist on both sides of region 1. They are the narrowest, and their colors are intermediate between those of regions 1 and 3.

The same result can be found in the MO image of the welded joint section. Region 1 is black and circled by a blank arc. Region 2 is between a red arc and the black arc, but is in light brown. Region 3 is the all orange area covering the outside of the red arc. Regions 1–3 respectively represent the WZ, the heat affected zone (HAZ), and base metal (BM). As the microstructure images show, there is a considerable amount of fine ferrites and pearlites in the WZ, whose distribution is dense and inhomogeneous. On the other hand, the grains in the HAZ are coarse and distributed inhomogeneously. The base metal area, consisting of ferrites and pearlites, is the largest of the three regions, and the ferrites and pearlites are distributed homogeneously.

Figure 6(a) was taken from the MO image of the welded joint section and was binarized. Then the pixels of row 40 were chosen to be the research object; hence figure 6(b) was acquired, revealing the change of gray scales. Figure 6(b) reveals the difference of microstructures clearly. It can be found that the curve is divided into three regions. In the WZ, it is divided into two relatively symmetrical parts along the dotted line; those gray scales decrease gradually from the central section and then fluctuate within a small range before reaching the HAZ. However, the graph width of HAZ is quite small owing to the rapid heating and solidification processes during laser welding, and its average gray scale exceeds the gray scale in WZ, though it is smaller than that of BM. As other curves that

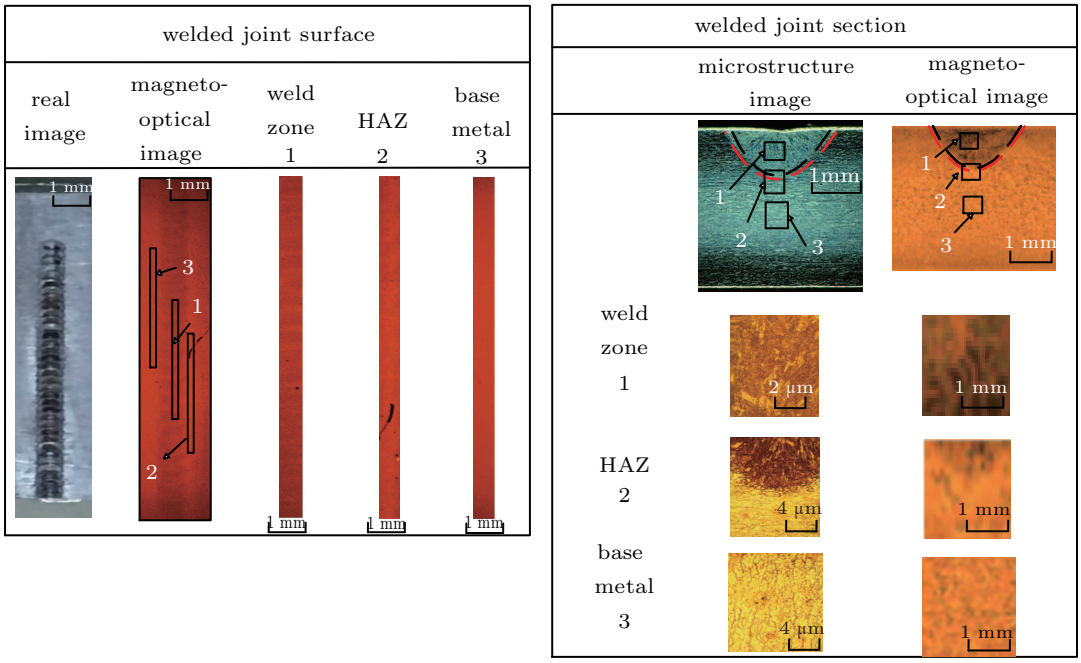


Fig. 5. (color online) Compared diagrams in different regions (1, 2, 3) of weldment A (the real image of the welded joint, magneto-optical images of the welded joint surface and section, partial selected image of welded joint surface in magneto-optical image, the microstructure image).

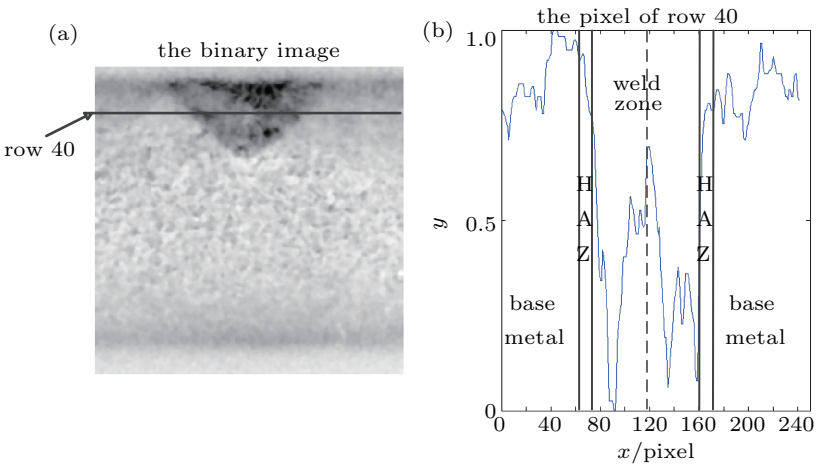


Fig. 6. (color online) Image processed diagrams of weldment A. (a) Binary image of weldment B. (b) Curve indicating the gray scales of row 40 in panel (a).

explain the change of BM appear to fluctuate within a stable and small range, the average gray scale in this region is the largest.

When the weldment was put into the magnetic field caused by the direct-current electromagnet, the weldment was magnetized. Then the direct-current electromagnet was taken away, and the residual magnetism B_r remained. Parameters B_{ra}, B_{rb}, and B_{rc} are defined as the residual magnetism of the WZ, HAZ, and BM, respectively. Parameters θ_a, θ_b, and θ_c represent the vibration angles of the incident light through the WZ, HAZ, and BM, respectively. Parameters I_a, I_b, and I_c are the light intensities of the analyzed light that passes through the WZ, HAZ, and BM, respectively. The following equations describe the relations of these parameters:

$$\theta_a = VB_{ra}L, \tag{7}$$

$$I_a = E^2\cos^2(\varphi + \theta_a), \tag{8}$$

$$\theta_b = VB_{rb}L, \tag{9}$$

$$I_b = E^2\cos^2(\varphi + \theta_b), \tag{10}$$

$$\theta_c = VB_{rc}L, \tag{11}$$

$$I_c = E^2\cos^2(\varphi + \theta_c). \tag{12}$$

Parameter S is defined as the grain size; S_a, S_b, and S_c are the grain sizes in the WZ, HAZ, and BM, respectively. As shown in Fig. 3, when S decreases, the hysteresis loop changes from curve 1 to 2 during demagnetization, and B_r increases. The size relation can be described as $S_a < S_b < S_c$, and $B_{ra} > B_{rb} > B_{rc}$. According to Eqs. (1), (7), (9), and (11), θ is proportional to B_r, hence $\theta_a > \theta_b > \theta_c$. Also, according to Eqs. (8), (10), and (12), the sum of φ and θ_b is less than $3\pi/2$, and E remains unchanged. Parameter I decreases while

θ increases; therefore $I_a < I_b < I_c$. The corresponding results are given in Table 3.

When an MO sensor is used to capture the MO image, the magnetic state of the magnetic medium is changed by the residual magnetic field in the weldment, and the Faraday rotation of the polarized light is induced. The change corresponds to the distribution of light intensity and shadow in the MO image. Since $I_a < I_b < I_c$, when the polarized light passes through the analyzer and is received by the image collector, the color of these regions gradually brightens and the gray scales increase from the WZ to BM as can be seen in Figs. 5 and 6. Finally, based on these results, the differences of microstructures in these regions can be calculated by using the MO sensor.

Another group of experiments for weldment B yielded similar results. A change in average power caused the thermal input to increase. As exhibited in Figs. 7 and 8, microstructures in the WZ grew along the weld centerline, perpendicular to the fusion line, and the grain size in this region was the smallest. The grain in the BM was larger than that in other regions. According to the theoretical analysis above, the curve that represents gray scale variation tends to increase from the WZ to BM; the color is black in the WZ, light brown in the HAZ, and orange in the WZ.

Table 3. Different B_r, θ, and I in the WZ, HAZ, and BM (S: small, M: medium, L: large).

	WZ(a)	HAZ(b)	BM(c)
S	S	M	L
B_r	L	M	S
θ	L	M	S
I	S	M	L

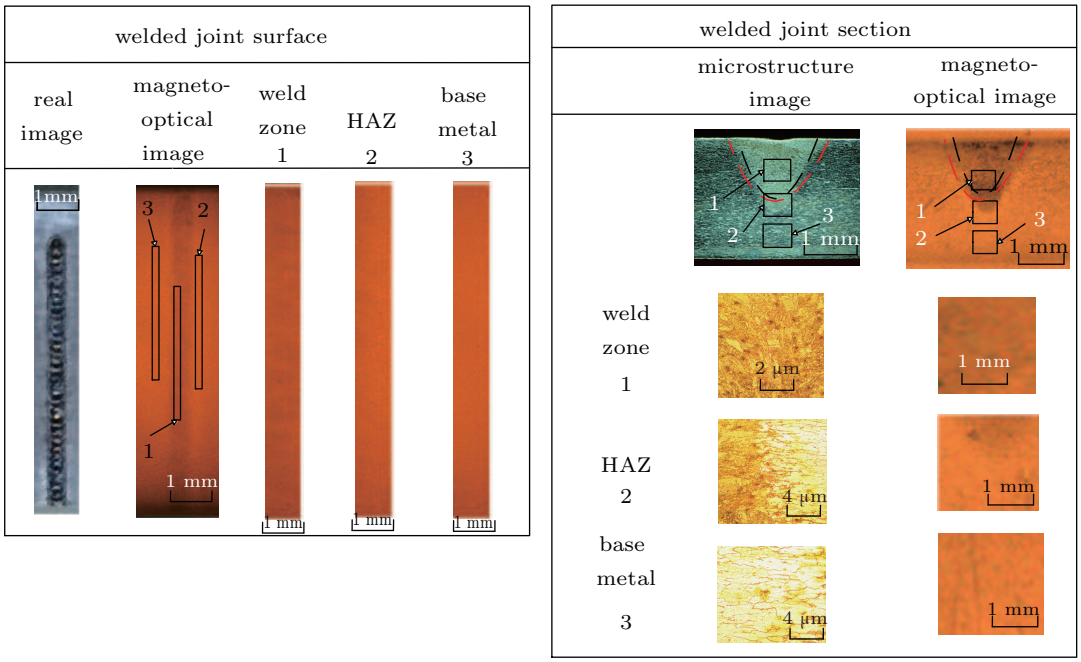


Fig. 7. (color online) Diagrams of different regions (1, 2, 3) of weldment B (real image of the welded joint, magneto-optical image of the welded joint section and surface, microstructure image).

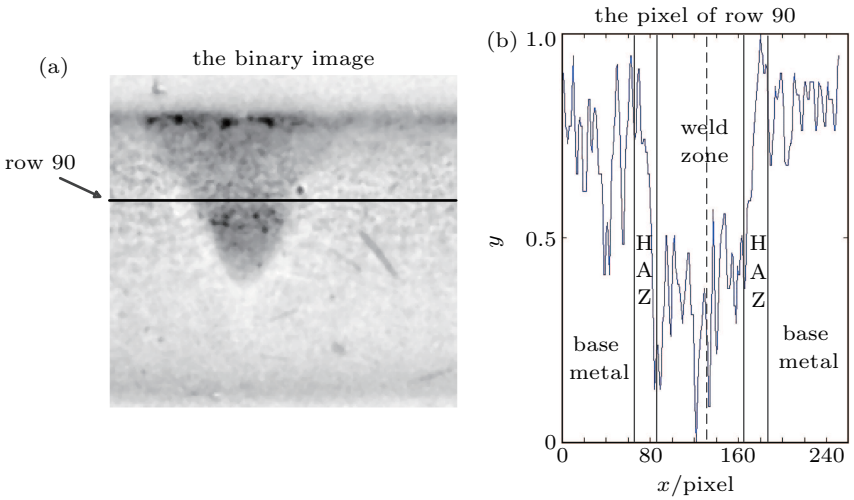


Fig. 8. (color online) Processed diagrams of weldment B images. (a) Binary image of weldment B, treated by the contrast stretched method. (b) Curve indicating the gray scales of row 90 of panel (a).

On the other hand, there are differences between weldment A and weldment B. When the average power changes for weldment B, the widths of WZ and HAZ increase, in which the thermal input is enhanced, unlike weldment A. During laser welding, microstructures are refined better at higher temperature, thus the grain sizes of weldment B are smaller than those on the corresponding regions of weldment A. According to the results in Table 3, when the grain size is smaller, the intensity of the acquired light is lower. Therefore the color in the MO images of weldment B is brighter, and the statistical average gray scale of each of its regions (BM, HAZ and WZ) is smaller too.

4. Conclusion

Two Q235 weldments, welded under different welding parameters, were studied. A novel microstructure detection method using the MO imaging technology was investigated. The main conclusions are as follows.

The grain size has a significant influence on the magnetism of electro-magnetic materials. The permeability of materials decreases and the coercivity increases as the grain size decreases. This makes the material hard to demagnetize, so greater residual magnetism remains.

Microstructure deformation obviously affects magnetism of materials. The key in material magnetization is the change of inner magnetic domain. High temperature causes some definite deformation of the microstructure of a welded joint during laser welding, which improves the rotational resistance of the magnetic moment and the domain wall, making it difficult to demagnetize the material.

The grain size increases from WZ to BM due to fast solidification, which is opposite to the changes of the residual magnetism in those regions. In optical-magneto imaging, the greater residual magnetism, the darker the color, and the larger the gray scales.

The grain size is closely related to the differences between MO images, and the corresponding relations between them are very helpful in identifying the differences in microstructure. Accordingly, MO imaging is an efficient method for microstructure inspection of welded joints.

References

[1] Gao X D, Wang R L, Long G F and Katayama S 2012 *Acta. Phys. Sin.* **61** 321 (in Chinese)
[2] Li S, Chen G and Zhou C 2015 *Int. J .Adv .Manuf .Technol.* **79** 177
[3] Zhang K, Lei Z, Chen Y, Liu M and Liu Y 2015 *Opt. Laser Technol.* **73** 139
[4] Qi M L, Zhong S, He H L, Fan D and Zhao L 2013 *Chin. Phys. B* **22** 377
[5] Sathish S, Mendik M, Cantrell J H and Yost W T 1995 *J .Acoust. Soc. Am.* **98** 2854
[6] Liu L, Liu X and Liu S 2006 *Scripta. Mater.* **55** 383
[7] Humphreys F J 2001 *J. Mater. Sci.* **36** 3833
[8] Ludwig W, Reischig P, King A, Herbig M, Lauridsen E, Johnson G, Marrow T J and Buffiere J Y 2009 *Rev. Sci. Instrum.* **80** 033905
[9] Gao X D and Chen Z Q 2015 *Chin. Phys. B* **24** 517
[10] Golubchik D, Polturak E, Koren G and Lipson S G 2009 *Opt. Express* **17** 16160
[11] Luo C P and Wang Y J 1993 *Acta. Phys. Sin. (Overseas Edition)* **2** 688
[12] He L X and Wang Y Z 2004 *Chin. Phy. B* **13** 754
[13] Weiss P 1901 *J. Phys. Theor. Appl.* **10** 556
[14] Lyuksyutov I F, Nattermann T and Pokrovsky V 1999 *Phy. Rev. B* **59** 4260
[15] Thompson S M, Allen P J and Tanner B K 1990 *IEEE T. Magn.* **26** 1984
[16] Hetherington M G, Jakubovics J P, Szpunar J A and Tanner B K 1987 *Philos .Mag. B* **56** 561
[17] Paul D I 1982 *J. Appl. Phys.* **53** 2362
[18] Ma G, Wu D, Niu F and Zou H 2015 *Opt. Laser. Eng.* **72** 39
[19] Xiang Y X, Zhu W J, Deng M X and Xuan F Z 2016 *Chin. Phys. B* **25** 229
[20] Joo S M, Bang H S and Kwak S Y 2014 *Int. J. Precis. Eng. Manuf.* **15** 447